Prediction of Aircraft-Propeller-Induced, Structure-Borne Interior Noise

James F. Unruh*
Southwest Research Institute, San Antonio, Texas

Coupled analytical and empirical structural-acoustic models of an aircraft fuselage and wing structure driven by propeller wake/vortex-induced loading are developed to predict structure-borne noise transmission into the aircraft cabin. Free-interface component coupling functions are used to couple the system components for structure-borne noise prediction. Predicted interior noise levels for the first two propeller tones are compared to laboratory-based test results to assess the predictive procedures. The results of the study indicate that accurate prediction of structure-borne noise transmission requires detail finite element modeling of wing panel motion.

Introduction

A POTENTIALLY important source of structure-borne interior noise transmission in propeller-driven aircraft is the interaction of the propeller wake and the aircraft wing structure.[1] The wing surface downstream of the propeller may experience significant aerodynamically induced fluctuating pressures due to the propeller wake, especially from the tip vortex.[2] In general, the level of propeller wake/vortex-induced, structure-borne noise (SBN) transmission in existing aircraft is unknown; however, empirical detection techniques have recently been reported that would allow estimation of this noise component.[3] Without an established data base from existing aircraft, estimation of propeller-induced SBN transmission in new generation aircraft will need to rely on analytical or semiempirical prediction methods.

This paper presents results from an evaluation of deterministic propeller-induced structure-borne noise transmission prediction as applied to a scale model aircraft fuselage and wing structure. The approach to the study was to evaluate the major structural-acoustic components individually to remove synergistic effects of component modeling errors. Detailed evaluation of coupled finite-element fuselage structural and cabin interior acoustic models of a test apparatus fuselage were reported in Ref. 4. The technique used to couple an analytical wing model to a fuselage empirical data base and the resulting model performance when subjected to propeller dynamic loading will be discussed in the sections to follow. The propeller-induced structure-borne noise empirical data used for model verification were acquired with the experimental apparatus shown in Fig. 1. A complete description of the test apparatus is given in Ref. 5. The major components of the test apparatus are a ring-stiffened fuselage shell with an integral floor and cabin acoustic trim, a fuselage acoustic shield to minimize airborne noise propagation, a wing structure for the structure-borne noise path, and a propeller source to provide wake-induced wing excitation.

Fuselage Structural/Acoustic Model

The model fuselage used in the validation study is a 72-in. long, 40-in. diam cylinder with 0.032-in. thick skin. The cylinder is stiffened by 18 evenly spaced stringers riveted to the cylinder skin. The stringers pass through eight internal ring frames spaced on 8.0-in. centers. The floor of the cylinder, 0.032-in. thick, is supported on continuous floor beams, extending across the ring frames at a distance of 11 in. below the cylinder center. Two longitudinal floor beams extend the length of the fuselage. The fuselage floor is bolted to the floor support beams and to the cylinder outer skin. The fuselage endcaps are 1/2-in. thick solid aluminum plate. The fuselage interior trim consists of a 1/2-in. thick fiberglass blanket on each endcap. Four layers of the same material completely line the walls of the cylinder, including the area below the floor. The cabin sidewall area is finished with a sheet of epoxy/fiberglass material 0.032-in. thick, and an additional 0.032-in. sheet of vinyl is used in a 120 deg sector as a headliner trim. The total weight of the fuselage is approximately 241 lb, with 125 lb being the solid aluminum endcaps.

In the wing-to-fuselage attachment structure, spherical bearings are used at each of the three attachment points to eliminate local moment transfer; only shear transfer is allowed. Overall wing moments are reacted by lateral differential shear in the front spar only. This physical arrangement confines the structure-borne noise transmission path to well-defined motions at the wing/fuselage attach points. Both the front and rear spar fuselage-to-wing attachments are directly secured to the fuselage floor beams and ring frames.

Empirical characterization of the fuselage with respect to SBN transmission from wing excitation was carried out in the frequency range from 100 to 500 Hz. This frequency range covers the first two dominant tones in the propeller speed

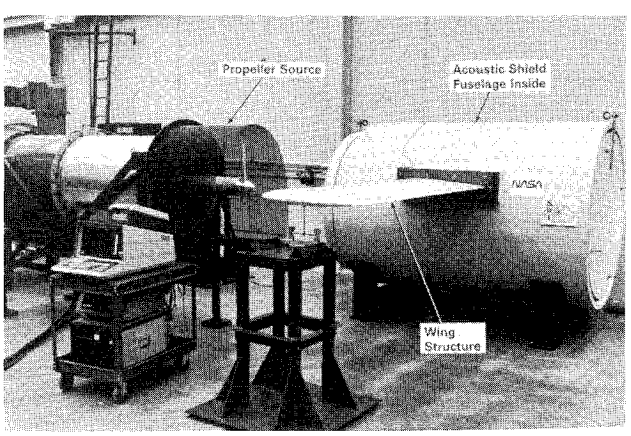

Fig. 1 Structure-borne noise test apparatus.

Received Oct. 29, 1987; revision received Jan. 4, 1988; presented as Paper 88-0267 at the AIAA 26th Aerospace Sciences Meeting, Reno, NV, Jan. 11-14, 1988.

*Staff Engineer, Department of Engineering Mechanics, Division of Engineering aned Materials Science. Senior Member AIAA.

range of interest, (3450 to 5700 rpm). The fuselage was supported on low-frequency mounts, while the wing attach points, two forward and one aft, were individually excited in the lateral (Y) and vertical (Z) directions. Acceleration responses at each excitation location and direction were recorded along with microphone responses at 12 interior cabin locations. A typical test setup configuration is shown in Fig. 2, wherein the drive is at wing-to-fuselage attach point location 2 in the Z direction. The upper-front spar wing-to-fuselage attachment is denoted as location 1, and the rear spar attachment is denoted as 3. As shown in Fig. 2, the 50 lb electrodynamic shaker used for excitation is acoustically shielded to prevent direct shaker airborne noise radiation to the fuselage. Acoustic pads were also used on the floor adjacent to the test article to reduce reflected standing waves that could influence the test results.

The electrodynamic shaker was driven with a swept sinusoid ramped from 80 Hz to 600 Hz within one-half the data analysis window. At the end of the "chirp," the current to the shaker-field coil was removed allowing system-free decay for the remaining time period. The chirp was repeated several times to allow sample averaging operations. Normally, seven to ten such averages are used to improve frequency response function definition. A 1.25 Hz analysis bandwidth was used in the spectral analysis of the data.

The scope of the data acquisition is best described in terms of generating a system inertance matrix, $[XI]$, as

$$\{a\} = [XI]\{F_F\} \tag{1}$$

where $\{a\}$ is the vector of wing-to-fuselage attach point accelerations due to the applied forces $\{F_F\}$ at the same wing-to-fuselage attach points, and wing attach point force to interior sound pressure response (SPL) matrix, $[TPF]$, for the form,

$$\{P\} = [TPF]\{F_F\} \tag{2}$$

where $\{P\}$ is the vector of interior microphone responses. With the shaker attached at wing-to-fuselage attach point 1, driving in the Y direction with all other attach points force-free, we may acquire frequency response functions corresponding to the first column of the inertance and interior SPL matrices. Likewise, by moving the shaker location or drive direction, all other elements of the system matrices were acquired. Detailed discussions and data presentations of the fuselage model may be found in Ref. 4.

Wing Structural Model

The wing structure is a 31.0-in. const chord NACA 0012 section airfoil with an exposed span of 80 in. The structure is of conventional sheet metal, and rivet construction, 0.040-in. skin and ribs on 16.0-in. centers. The wing front and rear spars, at 29 and 75% chord, extend an additional length of 13.5 in. beyond the skin surface to accommodate penetration through the fuselage acoustic shield used in the test apparatus. The wing weighs a total of 29.55 lb. The equations of motion for the wing structure take the form

$$[M]\{\ddot{u}\} + [C]\{\dot{u}\} + [K]\{u\} = [A]\{F_R\} + [B^T]\{F_W\} \tag{3}$$

where $[M]$, $[C]$, and $[K]$ are, respectively, the nodal dynamic mass, damping, and stiffness matrices of the assembled structure. The $[A]$ matrix transforms the externally applied loads $\{F_R\}$ into loads associated with the $\{u\}$ degree-of-freedom (DOF) set, and the matrix $[B]$ transforms the wing-to-fuselage attach point loads $\{F_W\}$ into loads associated with $\{u\}$. Generally, the $[A]$ and $[B]$ matrices are quite sparse and serve to select active DOF for the applied loads or loading interpolating weighting functions. For the purpose of reducing the total DOF involved in the coupling process, the wing nodal equations of motion were reduced to modal form, reflecting free constraints at the wing-to-fuselage attachments.[6] The resulting equations of motion may be written in modal form as

$$\begin{aligned}\lceil I \rfloor\{\ddot{q}_r\} + \lceil 2\beta_r\omega_r \rfloor\{\dot{q}_r\} + \lceil \omega_r^2 \rfloor\{q_r\} \\ = [\psi_r^T][A]\{F_R\} + [\psi_r^T][B^T]\{F_W\}\end{aligned} \tag{4}$$

where

$$\{u\} = [\psi]\{q_r\} \tag{5}$$

In the above expression ω_r and ψ_r are, respectively, the rth normal mode frequency and mode shape, and β_r is the corresponding equivalent critical viscous damping ratio.

Two wing structural dynamic models were generated, an equivalent elastic axis beam model,[7] and a detailed finite element model.[8] In the elastic axis beam model, elastic bending modes occurred at 87.8, 207, 513, 656, and 830 Hz with corresponding mode numbers 7, 11, 15, 17, and 20. Wing elastic torsion was quite pronounced, with several modes within the 830 Hz free-free mode frequency range. Wing fore and aft bending was quite stiff, with response just below the 830 Hz cutoff. For excitation in the vertical direction, wing fore-aft motion was not excited. For the free-wing model, the first six modes were nonelastic, rigid body modes.

The detailed finite-element model of the wing structure, shown in Fig. 3, consists of 26 rod elements, 119 beam

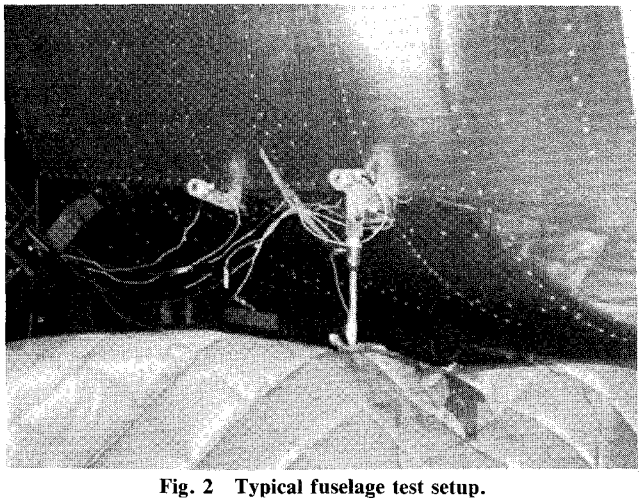

Fig. 2 Typical fuselage test setup.

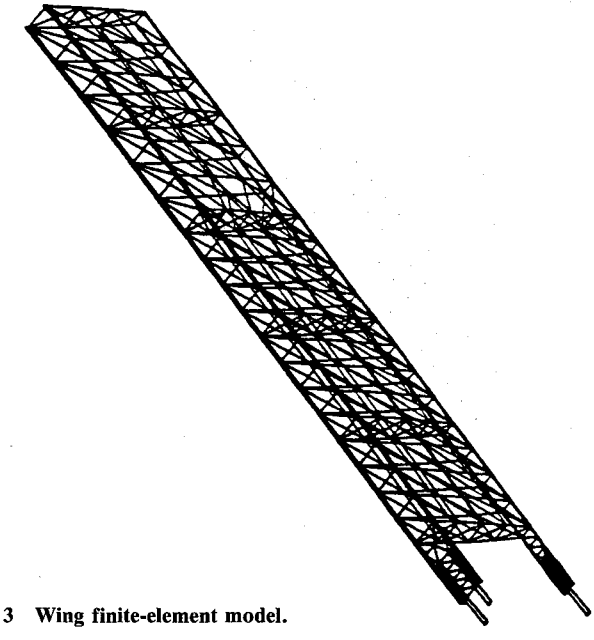

Fig. 3 Wing finite-element model.

elements, and 445 shell elements, for a total of 1374 dynamic DOF. The major skin panels between wing spars and rib sections are modeled as slightly curved panels, with 32 shell elements each. Both upper and lower wing panels were modeled. The structure forward of the wing front spar and aft of the wing rear spar was modeled as equivalent beams. Valid panel dynamic response is expected out through 200 Hz; beyond 200 Hz, the finite element panel grids lack sufficient definition. The panel effective cutoff range is quite dramatically shown in the modal density plot given in Fig. 4. As can be seen in Fig. 4, the number of elastic modes per frequency increment begins to decrease beyond 200 Hz and is dramatically reduced beyond 300 Hz. One-hundred normal modes of the structure were retained for the present evaluation; however, the first 80 modes were of primary interest. Wing mode shapes in this range were dominated by panel modes as shown in Fig. 5; however, overall bending modes were also well represented, as can be seen by the mode shape plots given in Fig. 6. It is of interest to note the first elastic wing bending mode in the finite element model is at 90 Hz, as compared to 87.8 for the beam model.

Coupled System

Two conditions at the wing-to-fuselage attach points must be met in order to insure proper coupling between the structural/acoustic fuselage and wing models.

1) The sum of attach point forces must vanish,

$$\{F_W\} + \{F_F\} = 0 \tag{6a}$$

2) The displacements at the attach points must be equal,

$$\{X_W\} = \{X_F\} \tag{6b}$$

where $\{F_W\}$ and $\{X_W\}$ are, respectively, the wing forces and displacements at the attach points to the fuselage; and $\{F_F\}$ and $\{X_F\}$ are, respectively, the fuselage attach point forces and displacements.

Upon inversion of the fuselage inertance matrix, we may express the forces acting at the fuselage in terms of the corresponding applied accelerations:

$$\{F_F\} = [XI]^{-1}\{a\} \tag{7}$$

and for harmonic motion, we may develop a relationship between the fuselage forces and attach point displacements,

$$\{F_F\} = -\omega^2 [XI]^{-1}\{X_F\} = [XS]\{X_F\} \tag{8}$$

where $[XS]$ is commonly referred to as the apparent stiffness matrix.

Application of the constraint conditions of Eqs. (6a) and (6b) to Eqs. (4) and (8) results in the system coupled equations of motion,

$$[I]\{\ddot{q}_r\} + [2\beta_r\omega_r]\{\dot{q}_r\} + ([\omega_r^2] + [\bar{K}])\{q_r\} = [\psi_r^T][A]\{F_R\} \tag{9a}$$

where the fuselage modal stiffness is defined as

$$[\bar{K}] = [\psi_r^T][B^T][XS][B][\psi_r] \tag{9b}$$

Upon solution for the modal responses $\{q_r\}$, the interior pressure responses are calculated as:

$$\{P\} = [TPF][XS][B][\psi_r]\{q_r\} \tag{10}$$

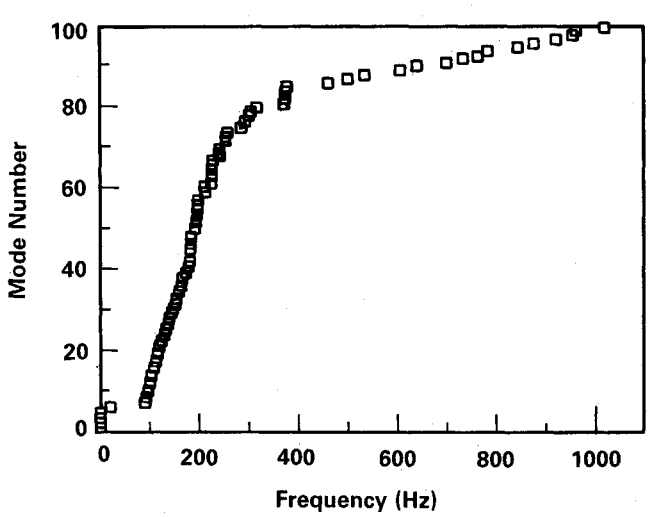

Fig. 4 Wing finite-element model modal density.

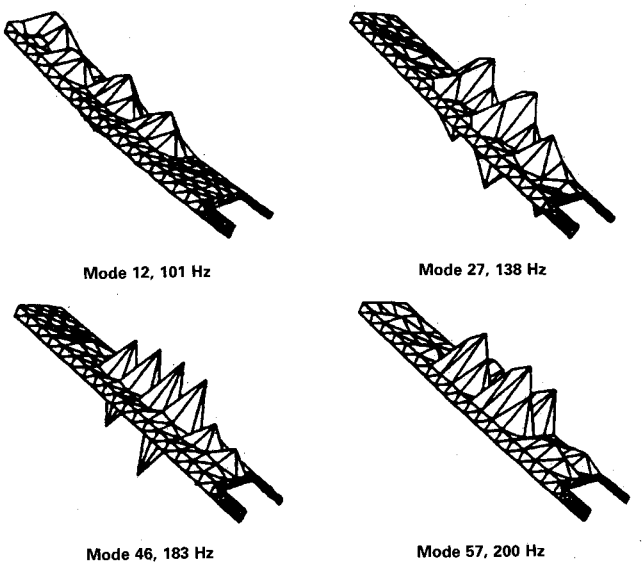

Fig. 5 Typical wing panel modes.

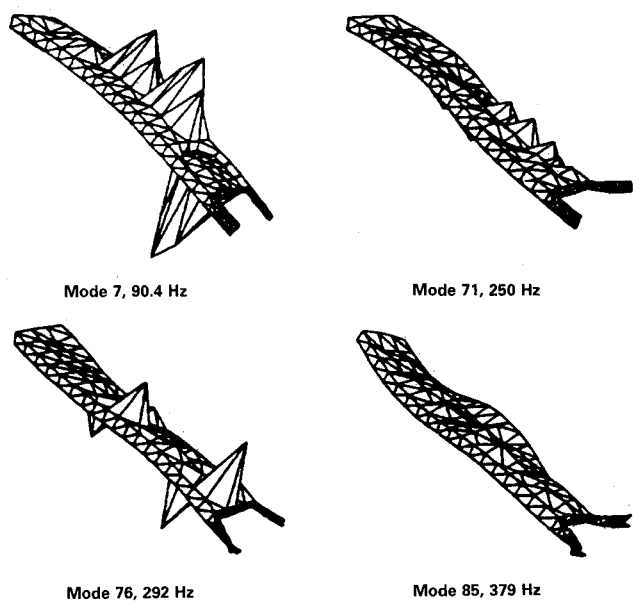

Fig. 6 Typical wing bending modes.

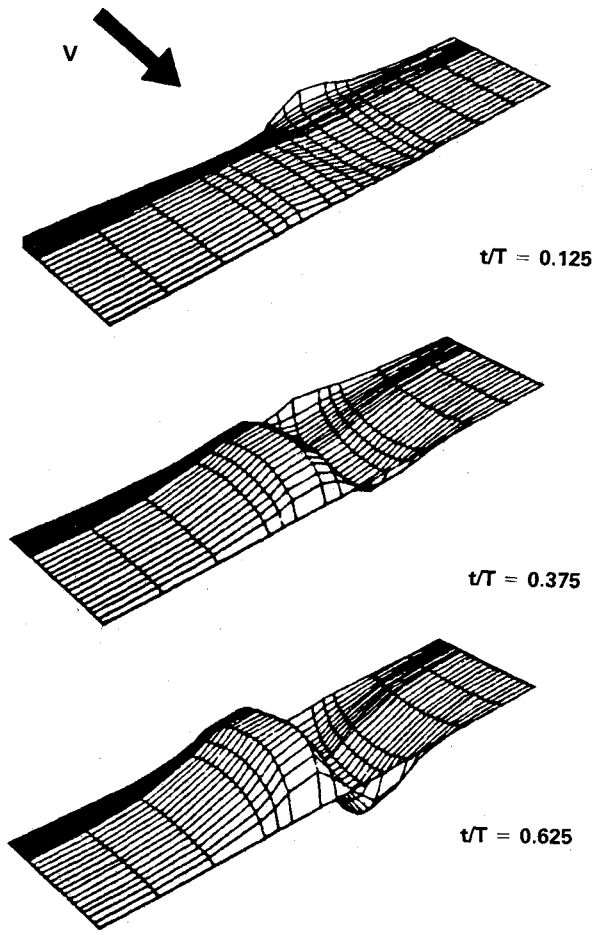

Fig. 7 Cyclic pressure loading with passage of the propeller, 4980 rpm.

With an estimation of the externally applied forces, $\{F_R\}$, the coupled equations of motion can be solved at the 1.25 Hz increments corresponding to the fuselage data base.

Wing Loading

Wing and interior noise responses were generated in the laboratory for wing excitation via an electrodynamic shaker attached to the wing front spar driving with a constant 1.0 lb rms force in the frequency range from 100 to 400 Hz and via propeller excitation at selected propeller speeds resulting in distinct excitations at propeller passing harmonics. The propeller source is a 28-in. diam, two-bladed propeller with a nearly constant 3-1/8-in. chord modified Clark-Y section. The propeller is powered by an 18 hp hydraulic motor with a maximum speed of 6000 rpm. A vane axial fan, powered by a 20 hp electric motor, provides a 33-in. diam, 70 ft/s inlet flow to the propeller to simulate forward flight. Thrust and torque curves for the propeller are given in Ref. 5.

To generate estimates of the propeller dynamic loading, the propeller wake is modeled by helical vortices shed from each blade tip. The Biot-Savart law is used to compute the normal velocity field generated by the downstream vortices. The velocity field is then imposed on a two-dimensional strip representation of the wing surface. Unsteady thin airfoil theory is then used to calculate the resulting surface pressures as if the wing were to produce such velocity deformations. The resulting unsteady pressure distributions are integrated across the wing surface panels to produce local lift and moments appropriate for loading the structural models. The procedures for developing the wing unsteady pressures are described in Ref. 9.

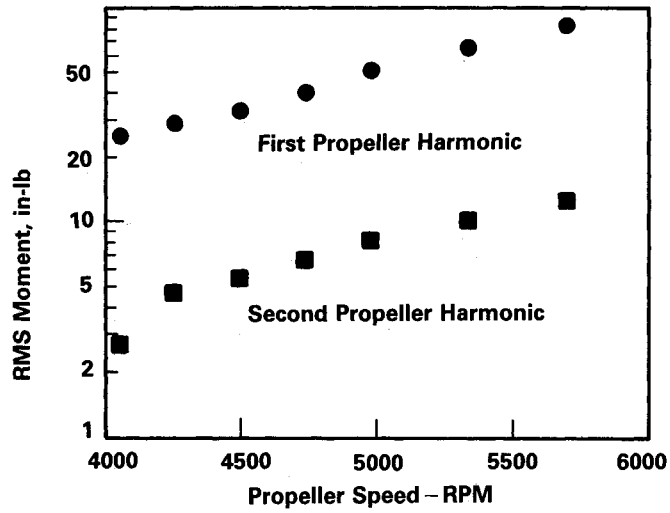

Fig. 8 Propeller-induced spanwise bending moments.

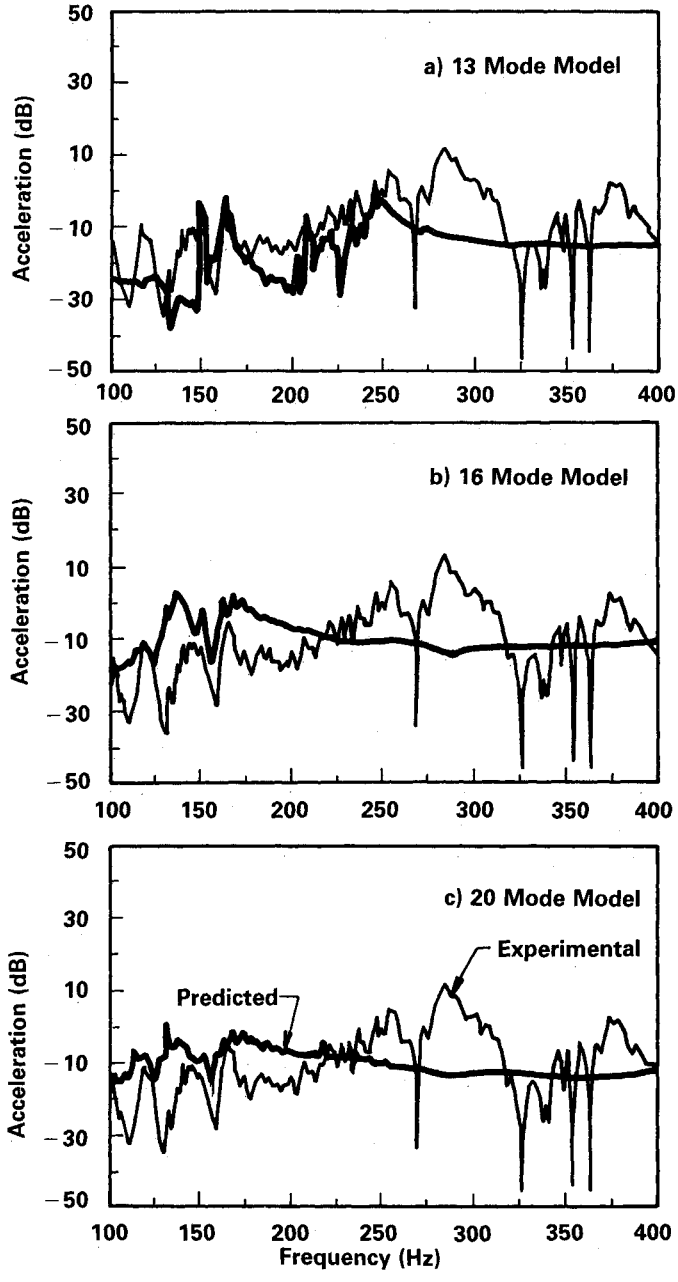

Fig. 9 Wing elastic axis beam models, acceleration response at shaker attach point, 1.0 lb rms at station 48.

Load estimates for several propeller harmonics at set propeller speeds were generated. It is of interest to note that the only significant loading within the first several propeller harmonics, insofar as overall induced forces, is a bending moment contribution about the propeller axis. This seems reasonable since the propeller tip vortex is convected onto the wind symmetrically. This is clearly seen by the typical pressure loading developed at various times during the propeller cyclic motion, as is given in Fig. 7. The magnitudes of the computed spanwise bending moments for the first two propeller harmonics for several propeller speeds are given in Fig. 8. These loads represent a propeller-to-wing leading-edge spacing of 1/4 the propeller diameter (7.0 in.) while the propeller axis lies in the wing chord plane.

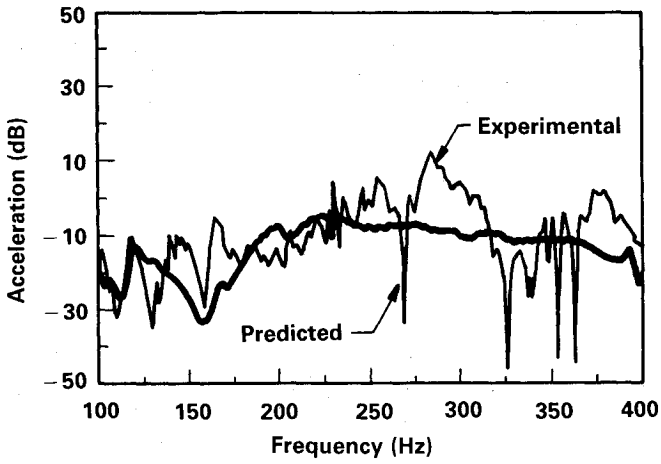

Fig. 10 Wing finite-element model acceleration response at shaker attach point, 1.0 lb rms at station 48.

Typical Results

The coupled system equations were driven with estimated loads duplicating the laboratory environment. In the predictions presented, a nominal 2% critical damping was assumed for all structural modes. Electrodynamic shaker excitation provided the most straightforward evaluation of the coupled models. The shaker was attached to the wing at station 48, which is at the second most inboard wing rib, and provided excitation in the frequency range 100 to 400 Hz. In Fig. 9, the resulting wing acceleration response at the shaker excitation point is shown for the beam wing model. Results from three models, using an increased number of wing normal modes, are given in Fig. 9 to indicate typical convergence requirements when using free-interface modal functions. In general, the measured acceleration response is much richer in character than the predictions reflecting wing panel and local shaker attach point compliance, which could not be accounted for in the beam model. Similar results, with some improvement, were found for the acceleration response predictions using the more detailed finite element wing model, as shown in Fig. 10. No attempt was made to "tune" the structural model to the measured results since it was felt that a majority of the discrepancy was due to local compliance effects at the shaker attachment point. Interior noise predictions for 2 of the 12

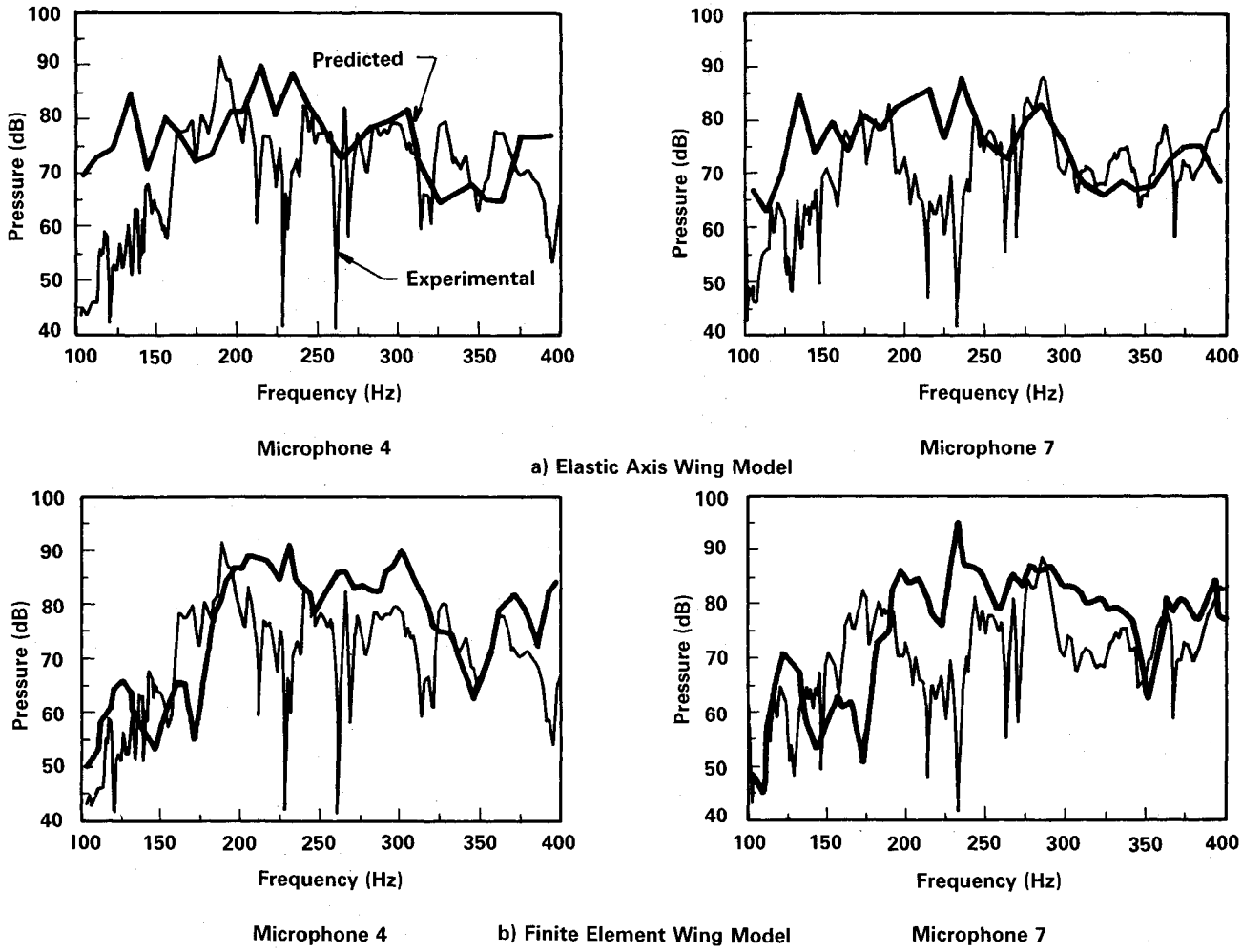

Fig. 11 Typical interior microphone response, shaker excitation 1.0 lb rms at station 48.

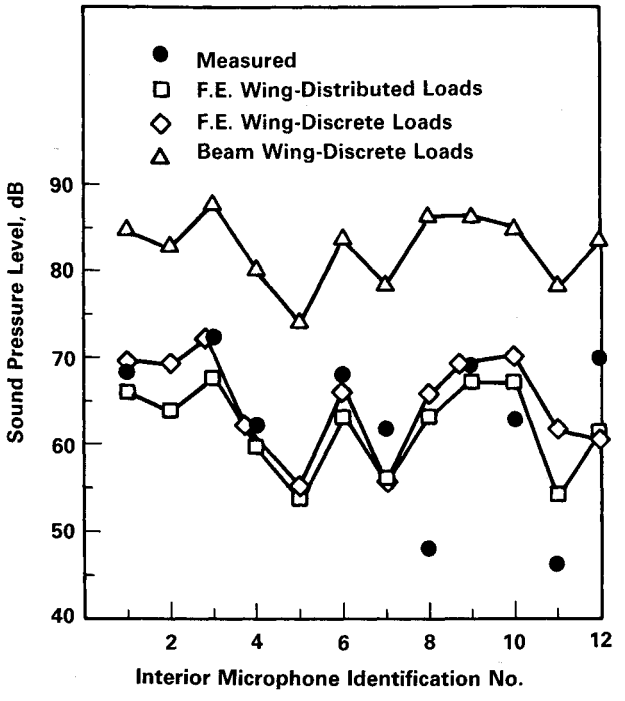

Fig. 12 Comparisons of predicted and measured interior noise levels at 4260 rpm (142 Hz).

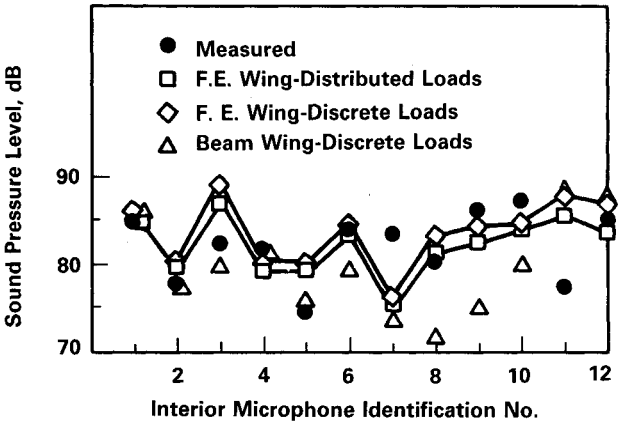

Fig. 13 Comparisons of predicted and measured interior noise levels at 4980 rpm (166 Hz).

cabin microphones are compared to measured results in Fig. 11. In Fig. 11a, results are given for the beam wing model, and in Fig. 11b results are given for the finite element wing model. The beam wing model SPL predictions are quite conservative out to approximately 175 Hz, as is the driving point acceleration. The finite element model improves the SPL predictions in the lower frequency range; however, neither model predicts the measured responses in the 200–250 Hz range, which is attributed to local shaker attach point compliance.

The finite element wing model was subjected to the distributed propeller loading corresponding to the first two propeller harmonics for several of the set propeller speeds. Likewise, the equivalent discrete moment loadings were applied to both wing models for a comparison on the effect of load distribution relative to structure-borne noise transmission and structural modeling requirements. The discrete moment loads were imposed on the wing front spar by applying a pair of out-of-phase forces about the propeller axis (Wing Station 64.0) at a distance of 16 in., which corresponds to adjacent wing ribs. In the propeller speed range from 4260 to 5700 rpm,

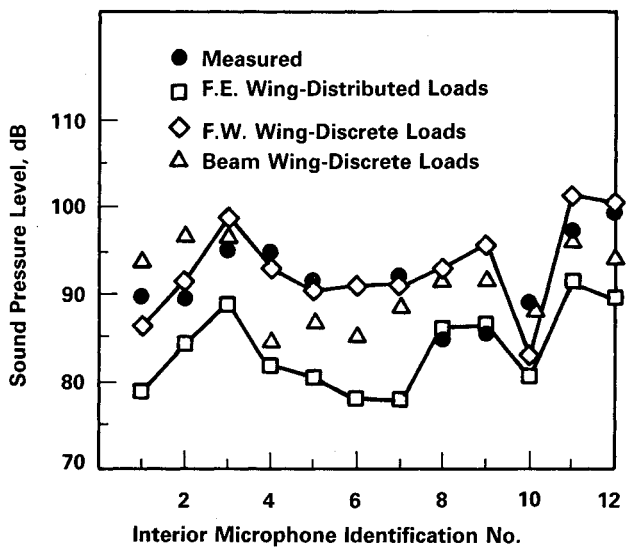

Fig. 14 Comparisons of predicted and measured interior noise levels at 5700 rpm (190 Hz).

the first propeller harmonic occurs in the 142 to 190 Hz range and the second propeller harmonic in the 284 to 380 Hz range. With the finite element wing model representing the wing structural characteristics reasonably well out to 200 Hz, reasonable interior noise predictions for the first propeller harmonic were expected. The propeller loading predictions at a given propeller speed were carried out at the harmonic center frequency, plus one frequency increment (1.25 Hz) on either side of the center frequency. The three response predictions were then energy averaged to give a band average value.

The sound pressure levels at 12 interior microphone locations were computed for three models: 1) the finite element wing model driven with distributed propeller loads, 2) the finite element wing model driven with discrete propeller moments, and 3) the elastic axis beam model driven with discrete propeller moments. The predictions for the first propeller harmonic response with comparison to laboratory measured data are given in Figs. 12–14 for propeller speeds of 4260, 4980, and 5700 rpm, corresponding to harmonics at 142, 166, and 190 Hz, respectively. The microphone locations within the test fuselage are of interest in interpreting the measured and computed results. A set of three microphones at equivalent passenger ear levels on the right, center, and left side of the cabin were used to record the interior noise levels. The microphone set was moved along the 72-in. cabin at set fuselage stations: 5, 26, 47, and 67. Microphones 2, 5, 8, and 11 are located on the cabin center line, which is at or near acoustic pressure node lines for several cabin normal modes.[5] The variation of measured sound pressure level throughout the cabin appears to decrease with increasing propeller speed. This reflects the increased modal density within the cabin and fuselage structures.[4]

The predictions for propeller speeds of 4260 and 4980 rpm show similar trends with good correlation of predicted and measured interior noise for the finite-element wing model with both the distributed and discrete propeller loading. Results for the 5700 rpm case (Fig. 14) show marked differences in predicted values between the distributed and discrete loading predictions for the finite-element wing model. The discrete loading predicts a majority of the measured interior levels reasonably well, while the distributed loading gives much lower interior levels. The discrete loading on the finite-element model appears to be the most consistent predictor of the propeller-induced interior noise. This can be more easily seen in the summary of overall spatial averaged (linear average of the 12 interior readings) interior noise levels given in Table 1.

Table 1 Summary of predicted and measured spatial average interior noise levels, dB, first propeller harmonic

	4260 rpm 142 Hz	4980 rpm 166 Hz	5700 rpm 190 Hz
Measured SPL	62.4	82.1	91.6
Finite-element wing distributed loads	62.0 (−0.4)	82.2 (+0.1)	83.7 (−7.9)
Finite-element wing discrete loads	65.0 (+2.6)	83.7 (+1.6)	93.1 (+1.5)
Beam wing discrete loads	82.2 (+19.8)	79.5 (−2.6)	91.2 (−0.4)

XX—Predicted SPL, (XX)—Measured minus predicted

Table 2 Summary of predicted and measured spatial average interior noise levels, dB, second propeller harmonic

	4260 rpm 284 Hz	4980 rpm 332 Hz	5700 rpm 380 Hz
Measured SPL	48.6	59.4	69.9
Finite-element wing distributed loads	68.5 (+19.9)	74.1 (+14.7)	75.6 (+5.7)
Finite-element wing discrete loads	71.8 (+23.2)	79.5 (+20.1)	81.8 (+11.9)
Beam wing discrete loads	70.4 (+21.8)	70.3 (+10.9)	80.3 (+10.4)

XX—Predicted SPL, (XX)—Measured minus predicted

Similar comparisons for the second propeller harmonics are summarized in Table 2. The results are consistently poor, and the measurements are significantly lower than the predictions. While it is realized that the finite element panel discretization breaks down beyond 200 Hz, such large differences were not expected.

One could visualize the wing structure as primarily a main beam front spar, with a series of discrete single DOF oscillators attached representing the various panel modal responses with the masses being driven by a series of discrete forces representing the various propeller harmonic loads. If the panel mass support springs were not sufficiently compliant, due to poor representation, then the propeller loads would transmit directly to the main spar. This could partially explain the overprediction of responses for the second propeller tone. On the other hand, to the author's knowledge, verification of the propeller loading predictions, via surface pressure or overall dynamic loads measurements, has not been carried out.

Conclusions

Coupled analytical and empirical structural acoustic models representing an aircraft fuselage and wing structure driven by propeller wake/vortex induced loading have been developed to predict structure-borne noise transmission into the aircraft cabin. Laboratory-based test results were used to verify the predictions procedures. The following conclusions may be drawn from this limited, but detailed, evaluation.

1) The use of coupled analytical and empirical models employing free-interface modal functions appears appropriate for structure-borne noise transmission prediction.

2) Wing structural modeling for accurate panel vibratory response beyond the first propeller harmonic for the laboratory-based test apparatus will require a substantial effort. In general, attention must be paid to accurate modeling of the wing panel dynamic response to obtain correspondingly accurate interior noise predictions for all propeller harmonics.

3) Propeller wake/vortex-induced loading predictions need to be verified directly via pressure or overall load measurements.

Acknowledgments

Financial support was provided by Southwest Research Institute Internal Research Panel, project No. 06-9415, and is truly appreciated. The author wishes to acknowledge the contribution of Mr. D. S. Weir of PRC Kentron, Inc. for supplying the propeller loading calculations and Mr. S. A. Dobosz for coding and carrying out the response solutions.

References

[1]Metcalf, V. L. and Mayes, W. H., "Structure-Borne Contribution to Interior Noise of Propeller Aircraft," Paper 830735, Business Aircraft Meeting and Exposition, Wichita, KS, April 1983.

[2]Miller, B. A., Duttman, J. A., and Jerachi, R.J., "The Propeller Tip Vortex—A Possible Contributor to Aircraft Cabin Noise," NASA TM 81768, April 1981.

[3]Unruh, J. S., "Test Procedures for Detection of In-Flight Propeller-Induced Structure-Borne Noise," AIAA Paper 87-0528, Jan. 1987.

[4]Unruh, J. F. and Dobosz, S. A., "Fuselage Structural-Acoustic Modeling for Structure-Borne Interior Noise Transmission," American Society of Mechanical Engineering, Paper 87-WA/NCA-15, Dec . 1987.

[5]Unruh, J. F., "Propeller-Induced Structure-Borne Noise: Laboratory Based Test Apparatus," AIAA Paper 86-1938, July 1986.

[6]Craig, R. R. and Chang, C. J., "Free-Interface Methods of Substructure Coupling for Dynamic Analysis," *AIAA Journal,* Vol. 14, Nov. 1976, pp. 1633–1635.

[7]Bruhn, E. F., *Analysis and Design of Flight Vehicle Structures,* Tri-State Offset Co., 1965.

[8]Bathe, K. J., *Finite Element Procedures in Engineering Analysis,* Prentice-Hall, Inc., 1982.

[9]Weir, D. S., "Wing Loads Induced by a Propeller Wake," AIAA Paper 86-1967, July 1986.